Heat and Mass Transfer 35 (1999) 65 – 73 © Springer-Verlag 1999

Experimental study on the pressure drop and heat transfer characteristics of tubes with internal wave-like longitudinal fins

B. Yu, J. H. Nie, Q. W. Wang, W. Q. Tao

Abstract Experiments were performed to determine the heat transfer and pressure drop characteristics in the entrance and fully developed regions of tubes with internal wave-like longitudinal fins. The test tube has a double-pipe structure, with the inner tube as an insertion. The wave-like fins are in the annulus and span its full width. Experiments were conducted for two cases: one with the inner tube blocked (no air flowing through it) and the other with the inner tube unblocked. The outer tube was electrically heated. Local and average heat transfer coefficients and friction factors were measured. The friction factor and Nusselt number correlations in the fully developed region were obtained in the Reynolds number range of 9×10^2 to 3.5×10^3. It has been found that the wave-like fins enhance heat transfer significantly with the blocked case being superior. In addition, the in-tube heat transfer process is characterized by an earlier transition from laminar to turbulent flow and Reynolds number-dependent thermal entrance length.

List of symbols

A	cross-sectional area of fluid flow
c	expansion length of the wave-like fin within annulus
c_p	specific heat of air at constant pressure
D_o	outer diameter of outer tube
D_i	inner diameter of outer tube
d_o	outer diameter of inner tube
d_i	inner diameter of inner tube
D_h	hydraulic diameter
F	heat transfer surface area, Eq. 4b
f	friction factor
h_x	local heat transfer coefficient
L	tube length
m	flow rate
N	number of waves
Nu_x	local Nusselt number
Nu	Nusselt number in fully developed region
p	static pressure
Q	heat transfer rate, Eq. 4a
Re	Reynolds number
T_b	air bulk temperature
T_{in}	inlet air temperature
T_{out}	outlet air temperature
T_w	wall temperature of outer tube
U_m	average velocity in the axial direction
x	coordinate in the direction of tube axis
δ	fin thickness
λ	thermal conductivity of air
η	fin efficiency
ν	kinematic viscosity
ρ	density

Subscripts

f	fin
r	root

Received on 12 May 1998

B. Yu, J.H. Nie, Q.W. Wang, W.Q. Tao
School of Energy & Power Engineering
Xi'an Jiaotong University Xi'an, Shaanxi 710049, P.R. China

Correspondence to: W.Q. Tao

This work was first supported by the Doctorate Fundation financed by the National Educational Committee of China (No. 9569801). Later, it was also supported by the National Natural Science Fundation of China (No. 59676019).

1 Introduction

The circular tube is one of the most widely-used heat transfer surface in heat exchangers, and the problem of enhancing the heat transfer rate in circular tubes has long been an important research subject. As an effective method for heat transfer enhancement, internally finned tube has been often employed in heat exchangers such as air compressor intercooler [1]. An internally finned tube usually should provide a significant surface area increase, e.g., 50% or more, and could offer an appreciable enhancement of heat transfer, ranging from tens to hundreds percentage. Many investigations, both experimental and numerical, have been conducted for different kinds of internally finned tubes [2–9]. Webb [1] made a detailed summary about this subject.

As far as the geometry of the internal fins is concerned, most internal fins are usually strips with flat surfaces positioned longitudinally along the tube axis. In some gas/liquid heat exchangers, however, gases flow inside the tube, and wave-like longitudinal fins (Fig. 1) are adopted to enhance the gas-side heat transfer process. To the best of the authors' knowledge, neither experimental measurements nor numerical analyses have been performed for such kind of internally finned tubes. The tube shown in Fig. 1(a) (type A) differs from that of

Fig. 1(b) (type B) in that the inner tube insertion of type B is fully blocked so that no flow goes through. This kind of enhanced tubes was recently adopted in air-water heat exchangers in Chinese factories. Air flows inside the tube while water flows across the tube. In the preliminary stage of its development, experimental tests were performed to find out the appropriate wave number. The overall heat transfer characteristics for tubes with wave number 8, 12, 18 and 20 were tested. Finally, the tube with wave number 20 is found to be the best in heat transfer performance under the design condition of the heat exchanger. Originally, the test tube was designed as that shown in Fig. 1(a), where the inserted tube was mainly served as a cartridge and was expected to have some enhancement effect. The work reported in [10] stimulated the present author to block the inserted tube so that only the annulus serves as an active heat transfer space. In [10] Fu and Tseng conducted an experimental investigation on the laminar flow and heat transfer of air in smooth tubes with and without an inner tube-insertion. They found that the heat transfer rate of the outer smooth tube could be increased appreciably by inserting the co-axial inner tube provided its size was not beyond a certain limit. Their numerical analysis also supports this observation [11]. The insertion of an appropriate inner tube makes more fluid flowing through the annular space, thus, the velocity gradient at the inner wall of the outer tube increases, leading to the enhancement of the heat transfer at outer tube surface.

In the present study, the two cases shown in Fig. 1 were carefully examined, using air as a working fluid. For the tube of type A, since the inner channel of the insertion is not blocked, its flow cross-section area only differs mildly from that without the insertion, with approximately 13% blockage. While for the tube of type B the cross-section of the inner tube is totally blocked, leading to an appreciable reduction in flow cross-section area. The major purposes of the study are: (1) to measure the pressure drop and heat transfer characteristics of the two tubes for both developing and developed flow region; (2) to compare the heat transfer performance of the two types of internally finned tubes, i.e., to clarify whether the blockage of the central insertion can enhance heat transfer.

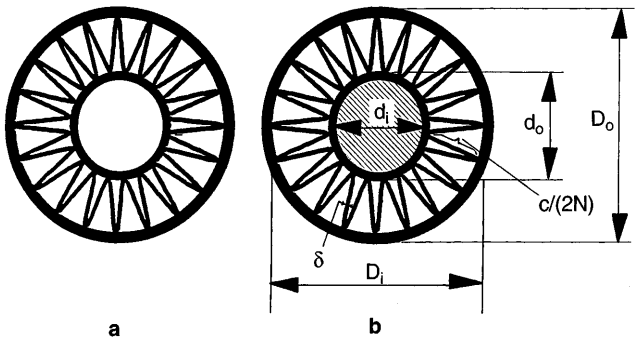

Fig. 1. Cross-section view of tube (**a**) unblocked (**b**) blocked

2
Experimental apparatus

The experimental apparatus is an open flow system with air as the working fluid as illustrated in Fig. 2. The test tube is arranged in such a way that its axis is in a horizontal plane. Under the influence of a downstream blower air first flows through a plenum chamber consisting of fine mesh screens to remove disturbance from the oncoming streams and make the fluid flow smooth. Downstream from the test tube is an after-duct with a mixing chamber for measuring the exit bulk temperature of the air. The flow rate can be adjusted by a by-pass valve.

The test tube and fins are made from copper. Its cross-sectional configuration is shown in Fig. 1. As seen there, the wave-like fins are within the annulus and span its full width. There are total 20 waves, each having an average length of c/N. The dimensions of the test tubes are shown in Table 1. When calculating the hydraulic diameters, the inner tube perimeters are taken into account since they are a part of the total wetted perimeters. The wave-like fins divide the annular space into two sections: one is the space between the fin and the inner surface of the outer tube which is referred to as side section. The other space locates between the fin and the inner tube and is referred to as center section.

Pressure taps were nonuniformly distributed in 13 cross-sections along the test tube axis (Fig. 3). There were 2 taps in each cross-section. One was installed in the center-section, and the other in the side-section (see Fig. 4). The temperatures of the test tube surface were measured by 39 copper-constantan thermocouples. They were also distributed in 13 cross-sections, each of which was placed at the middle between two successive pressure-tap cross-sections (Fig. 3). At each cross-section, three thermocouples were embedded equal-distantly along the outer surface (see Fig. 4). The thermocouple junctions were soft-soldered to grooves milled in the outer surface of

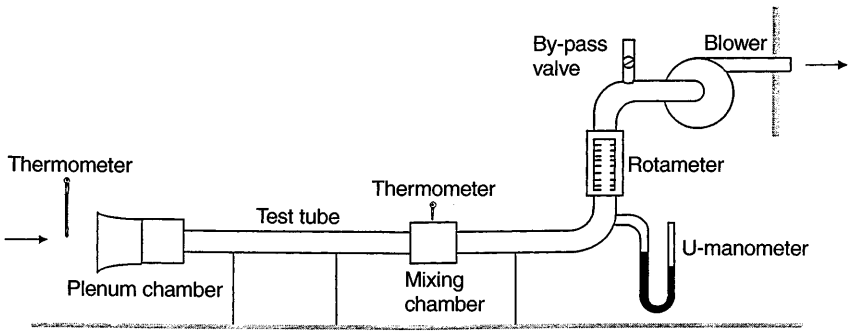

Fig. 2. Experimental apparatus

Table 1. Test tube geometry

Tube No.	case	L (mm)	c (mm)	D_o (mm)	D_i (mm)	d_o (mm)	d_i (mm)	δ (mm)	D_h (mm)
1	Unblocked	1000	390	35	33	11.5	10.5	0.25	3.10
2	Blocked	1000	390	35	33	11.5	10.5	0.25	2.84

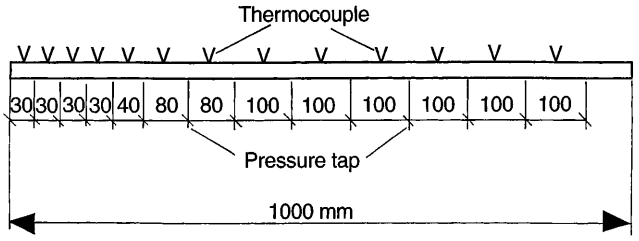

Fig. 3. Set up of thermocouples and pressure taps along tube axis

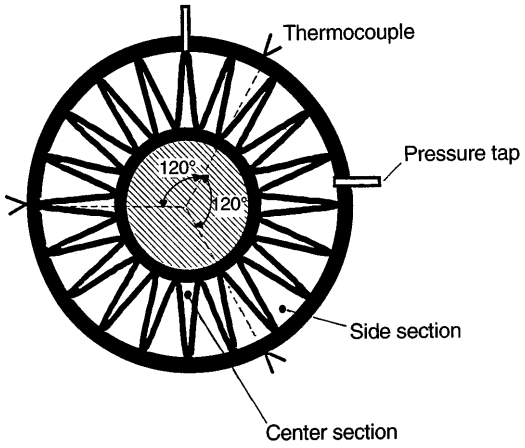

Fig. 4. Set up of thermocouples and pressure taps at a cross-section

the outer tube parallel to the tube axis. They were arranged to be flush with the tube surface. A layer of electrical insulation about 1 mm thick was employed to cover the tube surface, and the strip of the electrical heater was wound uniformly along the tube. The test tube was then thermally insulated by a 50 mm thick layer of thermal insulation.

The important measurements in these experiments include wall temperature, inlet and outlet air temperatures, air mass flow rate, static pressure and heat-generation rate. In the following paragraph the accuracy of these measurements will be presented.

As mentioned above 39 copper-constantan thermocouples were used to measure wall temperature. The accuracy of the thermocouple readings is estimated with $\pm 0.2^\circ$C. The inlet and outlet air temperatures were read from thermometers with a resolution of 0.1°C, and its accuracy is also about $\pm 0.20^\circ$C. The thermocouple junctions were installed to be flush with the outer surface of the copper duct, so the measured temperatures were not the inner surface values. Since the heat conductivity of tube wall is very high and thickness of the wall is quite small (1 mm), under the most unfavorable conditions heat conduction calculation indicates that the maximum temperature difference across the outer tube wall is less than 0.1°C. Thus the thermocouple readings are accepted as the wall temperature of the inner surface. The test section power input was measured by an electrodynamometer with a full-scale accuracy of 0.25 percent. Special measures were employed to minimize extraneous heat losses from the test section. These include good insulation between the test tube and the pre-duct and after-duct. The air flow rate was determined by a rotameter whose accuracy was 2.5 percent. The amount of heat transferred to the air flowing in the test tube could be determined from the mass flow rate of air and its entering and leaving temperature. The difference between the electric power input and the heat energy absorbed by the air was less than 5% for most cases, with the maximum difference of 7.2% . The pressure tap holes were 0.7 mm in diameter. The difference between the static pressure at each location tested and the atmospheric pressure was measured with an inclined manometer. The manometer accuracy was 0.1 mm water column. A barometer with an accuracy of 0.03% was used to measure the atmospheric pressure.

3
Data reduction and uncertainty estimation

The main purpose of the data reduction is to obtain Nu, f of the fully developed region and to find out a power-law correlation of Nu vs. Re, and f vs. Re for each tube. The average value of the entering and leaving air temperature was used to evaluate the physical properties of air. Hydraulic diameter was used as the characteristic length. The hydraulic diameter for the tube with blocked insertion was determined by

$$D_h = \frac{\pi(D_i^2 - d_o^2) - 4c\delta}{\pi(D_i + d_o) + 2c} \tag{1a}$$

while the case with unblocked insertion,

$$D_h = \frac{\pi(D_i^2 - d_o^2 + d_i^2) - 4c\delta}{\pi(D_i + d_o + d_i) + 2c} \tag{1b}$$

It should be noted that for this case since air flows in both the annulus and the inserted tube, their perimeters are all taken into consideration in the calculation of D_h.

The three important dimensionless parameters Re, Nu and f were defined as follows

$$\mathrm{Re} = \frac{U_m D_h}{\nu} \tag{2a}$$

$$\mathrm{Nu} = \frac{hD_h}{\lambda} \tag{2b}$$

$$f = -\frac{(\mathrm{d}p/\mathrm{d}x)D_h}{(1/2)\rho U_m^2} \tag{2c}$$

where the average velocity U_m was calculated from the measured volume flow rate of air and the calculated cross-section area for flowing air.

It was found that the static pressure values measured from the center section and the side section were almost the same. The maximum relative difference between the values measured from the two sections was no more than 5% . This fact indicates that although the two streams flowing in two separate subchannels are isolated by the fins, the air pressure of any cross-section may be considered as uniform, hence, only one distribution curve of pressure is needed to show the flow characteristics of the two streams. In the data reduction the average value of them was adopted.

The local heat transfer coefficient for the heated walls was defined here as

$$h_x = \frac{Q/F}{(T_w - T_b)} \tag{3}$$

where the convective heat transfer rate from the heated wall to the fluid, Q, was determined by

$$Q = mc_p(T_{out} - T_{in}) \tag{4a}$$

and the heat exchange surface area F was computed by

$$F = F_r + F_f\eta_f \tag{4b}$$

where

$$F_r = \pi D_i L \tag{4c}$$

$$F_f = 2cL + \pi d_o L \tag{4d}$$

The fin efficiency, η_f, was iteratively determined by the equation for rectangular fin during the data reduction, with $((c + \pi d_o)/(2N))$ as the fin height. As it can be seen from Fig. 4, each wave can be approximately regarded as two straight fins with height of $c/(2N)$, and attached at the inner surface of the outer tube. Here the outer surface of the inner tube is regarded as an extension of the fin in order to simplify the fin efficiency calculation. Since $\pi d_o/(2N)$ is much less that $c/(2N)$, this approximation is acceptable. This practice was adopted for both unblocked and blocked tubes. It is worth noting that for a comparison purpose, the heat exchange surface area of the two types of tube are taken the same. This means that the inner surface area of the inserted tube was not included for the unblocked case.

The local wall temperature T_w was the average value of the three thermocouple readings at the same cross-section. The local bulk temperature of the air at a cross-section located at a distance x from the duct inlet was determined by

$$T_b = T_{in} + \frac{Q \cdot x/L}{\rho c_p m} \tag{4e}$$

It is worth noting that the local temperatures measured by the 3 thermocouples at each cross-section were quite uniform, with a maximum deviation about 0.5°C, which was less than 5 percent of the difference of the local wall temperature and the local fluid temperature. Therefore the heated tube may be approximately regarded as being circumferentially uniform in temperature. It is usually expected that the local wall temperature where a fin is attached will lower or higher than bare surface. For our case, however, since the thermal conductivity of the base wall is very high (400 W/m.K) and the distance between two neighboring waves is quite small (5 mm). Thus the temperature of the envelope outer surface will be more or less uniform. An estimation for the axial heat conduction shows that for any case studied the heat transfer rate by the conduction through the tube wall is always less than 1% of the total heat transfer rate. Therefore an assumption is made in Eq. (4e) that the heat transfer rate is distributed linearly along the tube axis.

The heat transfer coefficient of the fully developed region was obtained by averaging $3 \sim 4$ successive local heat transfer coefficients in that region. The maximum relative deviation between them was usually within 4%.

An uncertainty estimation conducted along the lines suggested by Kline and McClintock [12, 13] shows that for a moderate flow rate (with Re = 1600–2000), the uncertainties in Re, f and Nu are about 3.5% , 4.6% and 5.8% respectively. For the case of the lowest flow rate, these uncertainties increase to 5.9, 7.6 and 9.3 percent. In the estimation, the uncertainty in physical properties was taken as 2%.

4 Results and discussion

4.1 Static pressure distribution along flow path

The first series of measurements were conducted to obtain pressure drop data for isothermal flow through the duct. The purpose was to find out the hydraulic entrance length and to determine the friction factor for the fully developed region.

Pressure distribution along the flow path of the two test tubes were measured in a range of Reynolds number from 9×10^2 to 3.5×10^3. Although this variation range of Reynolds number is not wide, it still covers the operation condition of most pressurized air intercoolers, which is usually around Re = 2×10^3. The variations of $P(0) - P(x)$ (in Pa) are shown in Fig. 5, with Reynolds number as a parameter, where $P(0)$ is the pressure at the entrance of the test section and $P(x)$ is the static pressure at the downstream station x. It can be observed clearly that after flowing a certain distance from the inlet, the fluid flow becomes fully developed, characterized by the linear variation of $(P(0) - P(x))$ with coordinate x. The entrance length of the flow developing region is about $40D_h$. In addition, the higher the Reynolds number, the larger the slope of the straight line. As far as the two types of tubes are compared, it can be seen that at the same Reynolds number air flow in blocked tube (type B) causes a bit more pressure drop than that in type A.

4.2 Friction factor in the fully developed region

The friction factors in the fully developed region are plotted as a function of the Reynolds number in Fig. 6, where the open circles represent the data of the unblocked tubes and the black circles correspond to the data of blocked tubes. At the same Reynolds number the friction

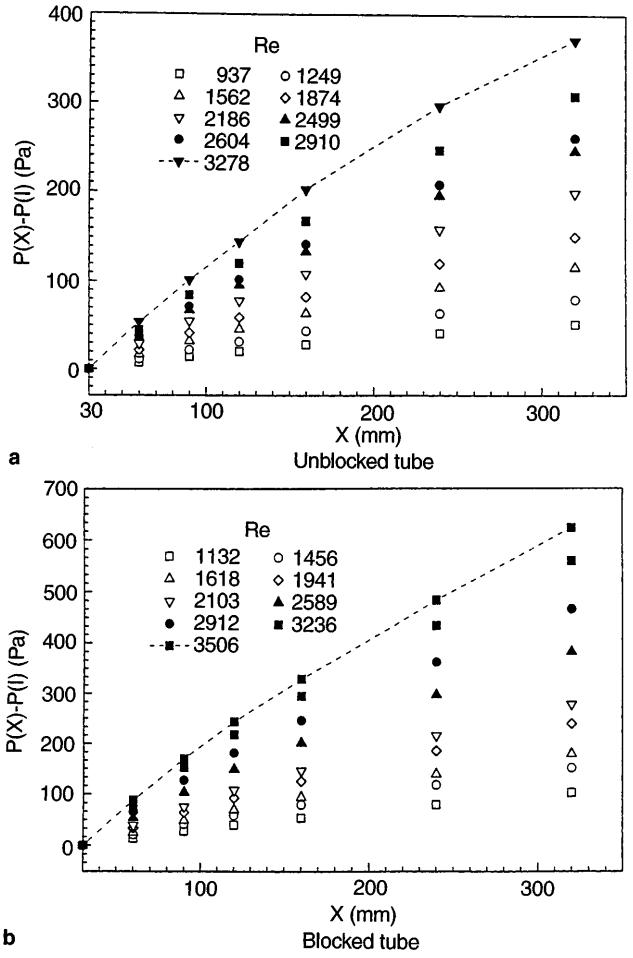

Fig. 5. Static pressure distribution (**a**) unblocked tube (**b**) blocked tube

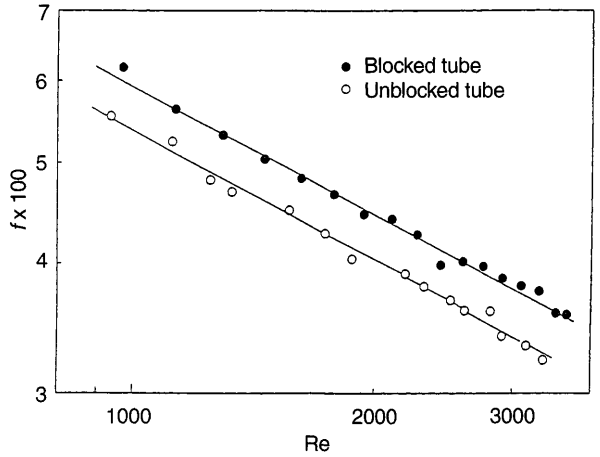

Fig. 6. Friction factor vs. Reynolds number

of the blocked tubes is about 12% higher than unlocked tubes. All the friction data for the two tubes were correlated. The results are presented below

for unblocked tube:

$$f = 0.971/\mathrm{Re}^{0.419} \quad (\mathrm{Re} = 930 \sim 3300) \tag{5a}$$

for blocked tube:

$$f = 0.991/\mathrm{Re}^{0.407} \quad (\mathrm{Re} = 970 \sim 3500) \tag{5b}$$

Attention is now given to the flow regime identification of the experimental data. As it can be see from Fig. 6, in the Reynolds number range studied (900 ~ 3300), all the friction factor in the fully developed region can be well-correlated by a power-law equation, indicating that these data may be considered in the same flow regime. the correlation is closer to the Blasius-type equation than to the form of f Re = const. Hence, we may considered that all the data (at least, most of the data) are in the turbulent flow region. The consideration will further be supported by the corresponding heat transfer data.

Some previous experimental results also show such kind of trend. i.e., the more complex the duct cross-section, the earlier the transition from laminar to turbulent. For example, Eckert and Irvine [14] found that the transition from laminar to turbulent flow occurred at Re = 1000 for a duct with triangular cross section of an apex angle of 11.5°. The observation of Xiao et al. [15] revealed similar character. In addition, it is worth noting that the hydraulic diameters of the test tubes are in the range of 2–3 mm. Although they can not be classified as micro-channel, but their dimensions are in its neighborhood. Experiments for micro-channels show that the smaller the tested tube, the earlier the transition from laminar to turbulent flow [16]. The above two ingredients, complicated cross-section and small hydraulic diameter, make the present authors to expect an earlier transition.

4.3 Local Nusselt number distribution

A series of runs were made at a variety of duct Reynolds numbers, in which the wall temperature distribution and the flow parameters were measured. In the data run, the heating current was applied to the duct, the desire air flow rate was set, and the test apparatus was allowed to operate until a steady-state condition was reached. A total of 31 runs were made. A summary of important measuremental results and operating conditions is presented in Table 2.

In the following the results of local Nusselt number will be presented first, followed by the average Nusselt number in the fully developed region.

The local Nusselt numbers for the heated surfaces have been determined at a succession of axial stations by employing the data reduction procedures described above. These results are presented in Fig. 7, where the Nusselt number is plotted against the axial coordinate x. Examination of the figures reveals the expected trend whereby higher Nusselt numbers correspond to higher Reynolds numbers. It has been found that for the unblocked tube, the local Nusselt number decreases gradually as x increases. For the blocked tube, the distribution of local Nusselt number at higher Reynolds numbers is different from that at lower Reynolds number. At higher Reynolds numbers there is a second summit at the location of about $25D_h$, and the higher the Reynolds number, the more apparent the second summit. While at lower Reynolds numbers the distribution

Table 2. Major measurement results and conditions

Run No.	m (kg/s)	Re	T_{in} (°C)	T_{out} (°C)	Total bulk temp. rise (°C)	Q (W)	Heat loss percentage (%)
	(blocked tube)						
1	0.00369	888	21.36	59.65	38.29	150.1	5.58
2	0.00441	1060	21.45	57.78	36.33	171.9	6.77
3	0.00504	1210	21.45	56.53	35.08	187.0	5.31
4	0.00573	1377	21.48	60.49	39.01	234.1	4.25
5	0.00576	1383	21.46	61.66	40.20	236.8	1.84
6	0.00638	1532	21.35	59.67	38.32	251.6	2.46
7	0.00703	1688	21.35	58.37	37.02	269.7	3.15
8	0.00764	1835	21.58	55.20	33.62	267.0	3.48
9	0.00822	1974	21.63	58.76	37.13	317.0	3.39
10	0.00841	2020	21.65	56.94	35.29	307.4	3.07
11	0.00940	2258	21.78	56.88	35.10	348.5	5.11
12	0.01071	2574	21.75	58.78	37.03	420.8	5.53
13	0.01080	2594	21.75	60.41	38.66	436.5	4.03
14	0.01181	2838	21.70	62.68	40.98	510.1	4.85
15	0.01334	3205	21.70	61.40	39.70	560.6	5.32
	(unblocked tube)						
1	0.00418	968	22.65	56.45	33.80	152.0	7.02
2	0.00475	1101	22.61	58.46	35.85	180.5	5.38
3	0.00553	1281	22.60	57.39	34.79	202.1	4.56
4	0.00617	1429	22.65	60.20	37.55	244.9	5.19
5	0.00654	1515	22.65	61.63	38.98	267.1	4.24
6	0.00735	1702	22.55	58.57	36.02	275.3	3.47
7	0.00799	1851	22.53	62.46	39.93	331.4	3.37
8	0.00887	2054	22.53	59.37	36.84	337.6	2.84
9	0.00937	2171	22.58	57.25	34.67	334.8	2.55
10	0.01045	2421	22.61	62.14	39.53	426.5	2.73
11	0.01096	2538	22.63	61.45	38.82	438.6	2.61
12	0.01163	2694	22.60	59.74	37.14	450.4	3.75
13	0.01227	2842	22.65	61.30	38.65	490.8	2.97
14	0.01301	3014	22.59	62.56	39.97	547.7	4.78
15	0.01372	3178	22.60	58.35	35.75	518.9	5.26
16	0.01406	3257	22.57	57.33	34.76	515.5	4.93

tendency is the same as the unblocked tube. The two different distributions of the local Nusselt number for the blocked tube meet at a Reynolds number around 1.6×10^3. The occurence of the second summit of Nu(x) distribution for the blocked case may be resulted from the flow seperation and reattachment at the entrance. Numerical simulation is now underway in the authors' group to reveal the mechanism of the phenomenon.

From Fig. 7 another feature may be noted. That is the thermal entrance length increase with the increase in Reynolds number. In the figure, a dashed line is dipicted to delineate approximately the two regions: thermal developing (left of the dashed line) and developed (right of the dashed line). This is qualitatively in good agreement with other experimental study of turbulent forced convection in ducts of non-circular cross-section [14]. In their experiments for a triangular duct with $D_h = 23$ mm, Eckert and Irvine found that at the lower Reynolds (< 5000) the local Nusselt number approaches a constant value at a duct location in excess of 70 diameter. However, when Re > 6000 the local Nusselt number never becomes constant but always decreasing over the range of x/D_h studied (~ 120). From the above discussion, it is obvious that for the tested tubes shown in Fig. 1 and Table. 1, which are characterized by a complex cross-section and a small hydraulic diameter, their heat transfer process is characterized by earlier transition from laminar to turbulent flow and Reynolds number-dependent thermal entrance length. More research work is needed in order to determine precisely the critical Reynolds number and thermal entrance region under different inlet conditions for such kind of complex duct. This project is now undertaken in the authors' group.

4.4 Nusselt number in the fully developed region

The variation of the Nusselt number vs. Reynolds number of the fully developed flow is shown in Fig. 8 for the two test tubes. Again, the open and black circles represent the unblocked and blocked test tubes, respectively. It is apparent that the two kinds of circles have a great gap between them. At the same Reynolds number the Nusselt number of the blocked tube is about 36% higher than that of unblocked tube and it has the tendency that as Reynolds number increases, the gap gradually increases. The Nusselt number data for the two cases were correlated separately. The correlated equations are as follows

for unblocked tubes:

$$\mathrm{Nu} = 0.00981\ \mathrm{Re}^{0.789} \qquad (\mathrm{Re} = 930 \sim 3300) \qquad (6a)$$

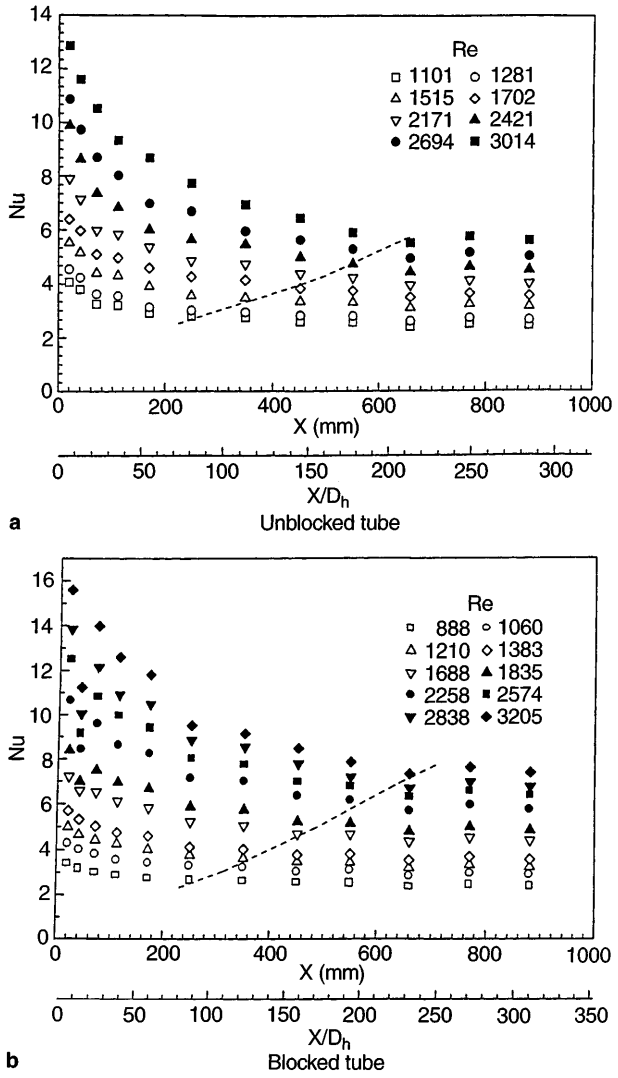

Fig. 7. Local Nusselt number distribution (**a**) unblocked tube (**b**) blocked tube

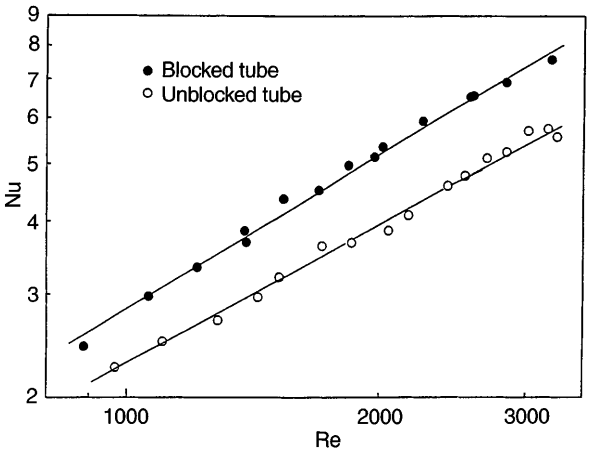

Fig. 8. Nusselt number vs. Reynolds number

for blocked tubes:

$$\mathrm{Nu} = 0.00668\ \mathrm{Re}^{0.876} \qquad (\mathrm{Re} = 880 \sim 3300) \qquad (6b)$$

The values of the two exponents in Eq. (6) are both near 0.8, which may be considered as another support to the flow regime identification described above.

4.5 Thermal performance comparisons

As indicated earlier, an internally finned tube usually could provide a significant increase in heat transfer. As for the two longitudinally finned tubes, we can find that at the same Reynolds number, the Nusselt number of the blocked tube is appreciably higher than that of the unblocked tube, while the friction of the blocked tube only has a mild increase. For example, for Re = 3300, the Nusselt number of the blocked case is about 36% higher than that of unblocked one, while the friction factor of the blocked case increases only 12% compared to the unblocked one. Hence, the blocked tube in test is advantageous to enhancing heat transfer. In order to appraise the thermal performance of the longitudinally finned tubes relative to the plane tube and evaluate the relative performance of the blocked finned tube over the unblocked one more precisely, comparisons were made under two conditions: 1. identical pumping power; 2. identical pressure drop. It can be shown that for these two constraints, following conditions must be met:

Identical pumping power:

$$(f\mathrm{Re}^3)_u = (f\mathrm{Re}^3)_b (A/D_h^4)_b \Big/ (A/D_h^4)_u \qquad (7a)$$

$$(f\mathrm{Re}^3)_u = (f\mathrm{Re}^3)_p (A/D_h^4)_p \Big/ (A/D_h^4)_u \qquad (7b)$$

Identical pressure drop:

$$(f\mathrm{Re}^2)_u = (f\mathrm{Re}^2)_b (1/D_h^3)_b \Big/ (1/D_h^3)_u \qquad (7c)$$

$$(f\mathrm{Re}^2)_u = (f\mathrm{Re}^2)_p (1/D_h^3)_p \Big/ (1/D_h^3)_u \qquad (7d)$$

where the subscripts "p", "u" and "b" refer to the plain tube, unblocked and blocked cases, respectively. In deriving Eqs. (7a) to (7d), the fluid properties are assumed to be constant.

The evaluation is proceeded in the following way. Selecting a Reynolds number for the unblocked case, the corresponding Reynolds number for the plain tube or the blocked case is determined from Eqs. (5a), (5b) and (7a) to (7c). Then from Nusselt number correlations (6a), (6b) and the Dittus-Boelter Equation, the ratio of heat transfer rate $(hF)_p/(hF)_u$, $(hF)_b/(hF)_u$ is obtained. The results are shown in Fig. (9a) and (9b), where the Reynolds number of unblocked case is taken as the abscissa. It can be seen that for the two constraints adopted, the performance of the two longitudinally finned tubes are much better than that of the plain tube, and the performance of the blocked tube is always superior to that of the unblocked one.

The significant heat transfer enhancement obtained from the two longitudinally finned tubes over the plain circular tube may be attributed to following three aspects. (1) The increase in heat transfer surface area of the finned tubes. For example, the total heat transfer surface area of

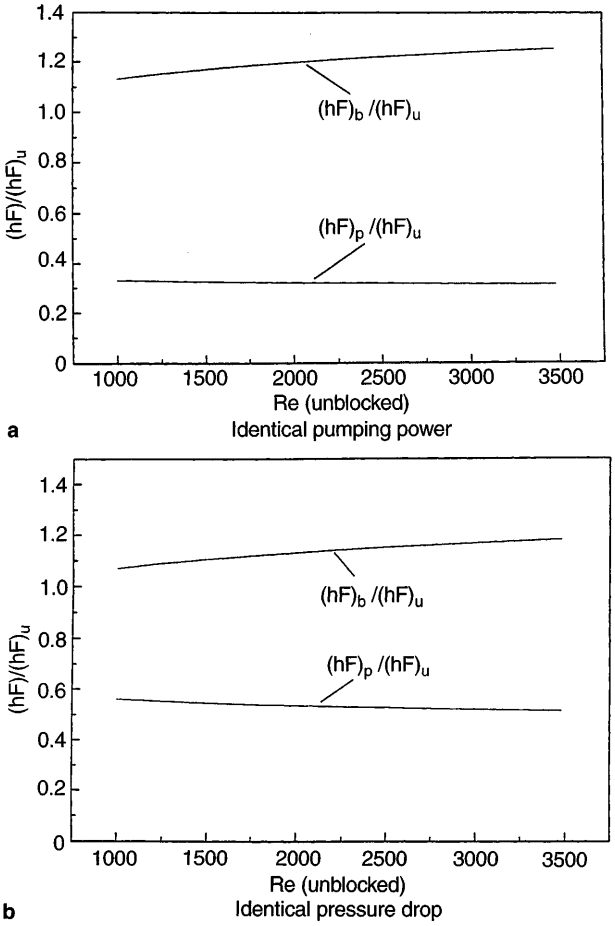

Fig. 9. Evaluation of thermal performance (**a**) identical pumping power (**b**) identical pressure drop

the blocked case is about 7.1 times of the smooth one with a fin efficiency of 0.9. (2) The reduction of hydraulic diameter, and (3) The insertion of the small central tube. Owing to the insertion of the inner tube, the flow rate in the annulus increases and hence the heat transfer in the annular space is enhanced. To clarify the role of the later two factors on the enhancement of heat transfer, comparison of the heat transfer performance was made between the blocked finned tube and a plain circular tube under the condition of identical mass flow rate. For this condition, following identify must be hold:

$$(A\mathrm{Re})_b = (A\mathrm{Re})_p (D_h)_b \Big/ (D_h)_p \qquad (8)$$

The results of $(hF)_b/(hF)_p$ vs $(\mathrm{Re})_b$ is shown in Fig. 10, It can be seen that the ratio of $(hF)_b/(hF)_p$ is larger than the surface area ratio F_b/F_p, indicating that the reduction in hydraulic diameter and the insertion of the central tube also contribute to the heat transfer enhancement quite appreciably.

5 Conclusions

In this paper, the pressure drop and heat transfer characteristics for both developing and developed regions of the tubes with wave-like internal longitudinal fins are, seemingly first in the literature, experimentally studied.

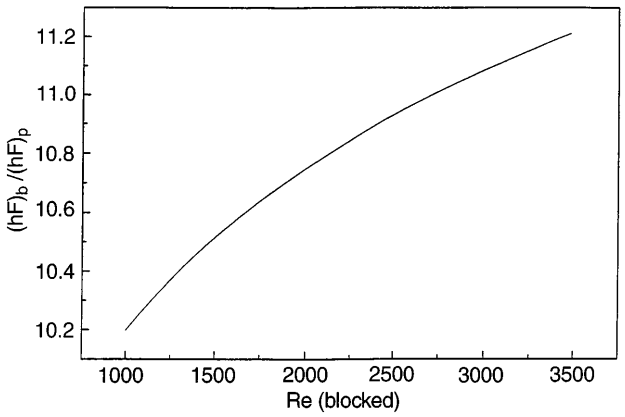

Fig. 10. Evaluation of thermal performance under identical mass flow rate

The friction factor and Nusselt number for the fully developed region in the Reynolds number range from 9×10^2 to 3.5×10^3 may be well-correlated by a power law equation, with exponents in $f \sim \mathrm{Re}$ and $\mathrm{Nu} \sim \mathrm{Re}$ about -0.4 & 0.8. This implies that for the tube configuration studied, the flow and heat transfer in the Reynolds number range $9 \times 10^2 \sim 3.5 \times 10^3$ may be regarded as in the turbulent region. Experimental results also show that the thermal entrance length is Reynolds number dependent. Thermal performance evaluation indicates that the two finned tubes can significantly enhance the heat transfer, with the blocked one being superior.

References

1. **Webb RL** (1994) Principles of Enhanced Heat Transfer, John Willey & Sons, Inc., New York
2. **Patankar SV; Ivanovic M; Sparrow EM** (1979) Analysis of Turbulent Flow and Heat Transfer in Internally Finned Tubes and Annulus. ASME J Heat Transfer 101: 29–37
3. **Webb RL; Scott MJ** (1980) A Parametric Analysis of the Performance of Internally Finned Tubes for Heat Exchanger Application. ASME J Heat Transfer 102: 38–43
4. **Tao WQ** (1987) Conjugated Laminar Forced Convective Heat Transfer from Internally Finned Tubes. ASME J Heat Transfer 109: 791–795
5. **Rustun IM; Soliman HM** (1988) Experimental Investigation of Laminar Mixed Convection in Tubes with Longitudinal Internal Fins. ASME J Heat Transfer 110: 310–313
6. **Kelkar KM; Patankar SV** (1990) Numerical Prediction of Fluid Flow and Heat Transfer in a Circular Tube with Longitudinal Fins Interrupted In the Streamwise Direction. ASME J Heat Transfer 112: 342–348
7. **Masliyah JH; Nandakumar K** (1976) Heat Transfer in Internally Finned Tubes. ASME J Heat Transfer 98: 257–261
8. **Lin MJ; Tao WQ; Lue SS** (1995) Study on Friction Factor of Developing and Developed Laminar Flow in Annular-Sector Ducts. J Thermal Science 4(3): 180–184
9. **Lue SS; Kang HJ; Lin MJ; Tao WQ** Experimental Study on Developed Turbulent Heat Transfer and Flow in Annular Sector Ducts, accepted by J Enhanced Heat Transfer for publication
10. **Fu WS; Tseng CC; Huang CS** (1995) Experimental Study of the Heat Transfer Enhancement of an Outer Tube with an Inner Tube Insertion. Int Heat Mass Transfer 38(18): 3443–3454
11. **Fu WS; Tseng CC** Enhancement of Heat Transfer for a Tube with an Inner Tube Insertion Int J Heat Mass Transfer (in press)

12. **Kline SJ; McClintock FA** (1953) Describing Uncertainties in Single Sample Experiments. Mechanical Engineering 75: 3–8
13. **Kline SJ** (1985) The Purpose of Uncertainty Analysis. ASME J Fluids Engineering 117: 153–160
14. **Eckert ERG; Irvine Jr TF** (1960) Pressure Drop and Heat Transfer in a Duct with Triangular Cross Section. ASME J Heat Transfer 83: 125–136
15. **Xiao Q; Chen B; Tao WQ** (1992) Experimental Study on Effect of Interwall Tube Cylinder on Heat Transfer of Corrugated Plate Fin and Tube Heat Exchanger. ASME J Heat Transfer 114: 755–758
16. **Peng XF; Wang BX** (1994) Liquid Flow and Heat Transfer in Micro Channels With/Without Phase Change. Proceedings of the 10th International Heat Transfer Conference. Brighton UK 1: 159–178